



## Serpentinization of the martian crust during Noachian

Yoann Quesnel<sup>a,b,\*</sup>, Christophe Sotin<sup>c,d</sup>, Benoit Langlais<sup>d,e</sup>, Simona Costin<sup>f</sup>, Mioara Mandaia<sup>a</sup>, Matthias Gottschalk<sup>a</sup>, Jérôme Dymont<sup>g</sup>

<sup>a</sup> GeoForschungsZentrum Potsdam, Telegrafenberg, 14473 Potsdam, Germany

<sup>b</sup> CEREGE, Europôle de l'Arbois BP80, 13545 Aix-en-Provence cedex 04, France

<sup>c</sup> Jet Propulsion Laboratory, California Institute of Technology, Pasadena, California, USA

<sup>d</sup> CNRS, UMR 6112, Laboratoire de Planétologie et Géodynamique de Nantes, 2, rue de la Houssinière, 44322 Nantes, France

<sup>e</sup> Université de Nantes, Laboratoire de Planétologie et Géodynamique de Nantes, 2, rue de la Houssinière, 44322 Nantes, France

<sup>f</sup> Department of Geological Sciences, University of Saskatchewan, 114, Science Place, Saskatoon, S7N 5E2, Canada

<sup>g</sup> Institut de Physique du Globe de Paris, Géosciences Marines, 75252 Paris, France

### ARTICLE INFO

#### Article history:

Received 14 January 2008

Received in revised form 13 October 2008

Accepted 17 October 2008

Available online 21 November 2008

Editor: T. Spohn

#### Keywords:

Mars  
serpentinization  
dichotomy  
magnetization  
Noachian  
early evolution  
magnetite

### ABSTRACT

This paper proposes a model of serpentinization of the Southern martian crust that may explain the topographic dichotomy, the absence of an associated free-air gravity anomaly and the presence of strong magnetic anomalies in the Southern Hemisphere. The thermodynamical conditions for serpentinization were likely met in the lithosphere during the Noachian period. This process may have decreased the density in the Southern crust and created the topographic dichotomy. Different reactions of serpentinization that can form magnetite have been considered. Assuming an intense magnetic field (core dynamo), we obtain chemical remanent magnetizations that are in the order of the estimates deduced from martian magnetic anomaly studies. The pertinence and the implications of our model concerning the early thermal evolution of Mars are discussed, with emphasis on the intensity of the paleo-magnetic field.

© 2008 Elsevier B.V. All rights reserved.

### 1. Introduction

Most of the processes that shaped Mars occurred during the Noachian era (4.5–3.7 Ga). The martian dichotomy – between a cratered, high and magnetic Southern Hemisphere and a flat, low and demagnetized Northern Hemisphere (Fig. 1) – was probably formed during this period. Most of the magnetic anomalies revealed by the MAGnetometer/Electron Reflectometer (MAG/ER) experiment onboard the Mars Global Surveyor (MGS) probe are predominantly distributed in the Southern Hemisphere over Noachian surfaces, which argues in favor of a global dynamo field that ceased before the end of this period (Acuña et al., 2001). To explain the absence of magnetic anomalies over the Northern Hemisphere, the origin of this dichotomy has to be investigated. Exogenic (crustal thinning by one or several impacts) and/or endogenic (degree-1 mantle convection) were suggested (see Watters et al., 2007 and references therein). Via a single or several long-lived hot plumes, the growth of the Tharsis volcanic province was probably initiated during Noachian (Roberts and Zhong, 2007; Solomon et al., 2005). Some of its

associated volcanic units are then emplaced on old magnetized crust, whereas others may have erased the crustal magnetization during their post-dynamo emplacement. A key issue is then to propose a scenario that explains all these planetary-scale geological features, considering the timing of the cessation of the core dynamo.

This can be investigated by studying the crustal magnetic field anomalies observed by the MGS MAG/ER instrument. Models dealing with the martian crustal magnetization predict intense and deep sources, in comparison with the Earth's crustal magnetization (Langlais et al., 2004; Quesnel et al., 2007; Whaler and Purucker, 2005). This gives some information about the material and the geological processes involved in this remanent magnetization. Before presenting the arguments which favor magnetite (Fe<sub>3</sub>O<sub>4</sub>) as main magnetization carrier, we review other potential candidates. Pyrrhotite (FeS) was suggested because it was observed in SNC meteorites; it also explains the apparent demagnetization of impact basins (Rochette et al., 2001). Pyrrhotite would imply a relatively thin magnetized layer due to its low Curie temperature. Multi-domain hematite (Fe<sub>2</sub>O<sub>3</sub>) was also invoked because it can be associated with large TRM (Kletetschka et al., 2000, 2005). However, the localized hematite spherules of Sinus Meridiani are mostly composed of single-domain hematite (Morris et al., 2005), associated with much lower magnetization. Furthermore, hematite minerals are more readily

\* Corresponding author. CEREGE, Europôle de l'Arbois BP80, 13545 Aix-en-Provence cedex 04, France. Tel.: +33 442971562; fax: +33 442971595.

E-mail address: [quesnel@cerege.fr](mailto:quesnel@cerege.fr) (Y. Quesnel).

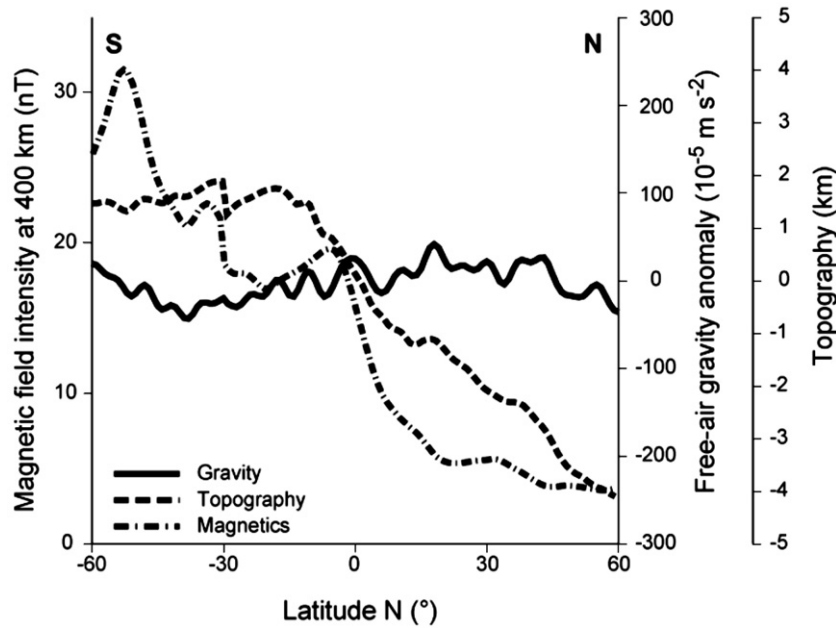


**Fig. 1.** Average profiles of martian topography, free-air gravity anomaly and 400 km – altitude magnetic field intensity signals across the dichotomy between  $-60$  and  $60^\circ\text{N}$ . Each profile corresponds to 121 values with 1 degree interval. These values were computed at each latitude by summing the values of each longitude (1 degree interval), divided by 360, using the Mars's topography, gravity and magnetic field models of Smith et al. (1999), Yuan et al. (2001) and Langlais et al. (2004), respectively. Values above Hellas and Argyre impact basins were not taken into account. The scale for the free-air gravity anomaly is in  $10^{-5} \text{ m s}^{-2}$ , i.e. in mGal.

weathered compared to magnetite. In conclusion, magnetite appears to be the most serious candidate as magnetization carrier (Dunlop and Arkani-Hamed, 2005). Together with maghemite, its oxidation product, it composes most of the magnetic phase on soils and rocks of Spirit landing sites (Bertelsen et al., 2004). Its high Curie temperature and its stable remanence may also explain the large magnetization depths derived from MGS magnetic measurements (Arkani-Hamed, 2005; Quesnel et al., 2007).

The preferred martian crustal magnetization mechanism is thermo-remanent magnetization (TRM): minerals cool below their Curie temperature in the presence of a dynamo field during seafloor spreading (Connerney et al., 1999), successive dike intrusions (Nimmo, 2000), or impacts (Connerney et al., 2001). This TRM can be thereafter modified by demagnetization associated with volcanoes or impact craters taking place after the cessation of the dynamo (Nimmo and Gilmore, 2001). Viscous remanent magnetization and demagnetization of the lower crust were also suggested by Arkani-Hamed (2007) and Shahnas and Arkani-Hamed (2007). Finally, Chemical Remanent Magnetization (CRM) processes may have generated the observed magnetic field anomalies. For instance, the alteration of siderite ( $\text{FeCO}_3$ ) into magnetite through magmatic intrusion in a water-rich crust can induce a secondary TRM and produce water discharges that could explain the apparent correlation between valley networks and magnetic anomalies (Harrison and Grimm, 2002).

An alternate model may be crustal CRM associated to serpentinization. This metamorphic reaction corresponds to the hydration of mafic minerals, generally producing serpentinite ( $\text{Mg}_6\text{Si}_4\text{O}_{10}(\text{OH})_8$ ) and other minerals such as magnetite, talc ( $\text{Mg}_3\text{Si}_4\text{O}_{10}(\text{OH})_2$ ) or quartz ( $\text{SiO}_2$ ). Dihydrogen ( $\text{H}_2$ ) is also produced and methane ( $\text{CH}_4$ ) can eventually be formed if the reactant fluid contains carbon dioxide ( $\text{CO}_2$ ). Serpentinization occurs at relatively low pressures ( $<400 \text{ MPa}$ ) and low to medium temperatures ( $<600 \text{ }^\circ\text{C}$ ). On Earth, serpentinization sites are commonly found at mid-ocean ridges, transform faults and passive margins, where shallow peridotitic mantle rocks are exhumed (Mével, 2003). Another setting is the mantle wedge of subduction where water is released from the subducted crust. In the presence of an intense magnetic field, the production of magnetite allows the mafic or ultramafic serpentinized rock to be chemically

magnetized. The resulting magnetic anomalies can be large enough to be mapped at satellite altitudes on Earth (Blakely et al., 2005). Finally, serpentinization increases the rock volume, creating a relief with surrounding non-serpentinized rocks (e.g. mid-ocean ridge elevation model of Hess, 1962).

In this paper, we investigate the serpentinization of the Noachian martian crust to explain the observed magnetic anomalies. We first describe the reference crustal model in terms of temperature and composition as regards the gravity signal. Further we compute the expected magnetizations obtained via serpentinization. These values are compared with the martian crustal magnetization models derived from MGS measurements. In the last part we discuss our evolution model and the new insights it brings on the early Mars, especially with respect to the paleomagnetic field.

## 2. Thermal and compositional crustal model for early Mars

### 2.1. Early evolution and thermal gradient

Based on simple considerations about the energy released by the growth process, the temperature of the martian outer crust was high during accretion since a magma ocean was likely present. The depth extent of this magma ocean is not well-constrained (Reese and Solomatov, 2006). Just after accretion, the temperature is controlled by the melting of iron and silicate phases and their subsequent cooling. This is followed by the onset of convection in the mantle (Korenaga and Jordan, 2002), which quickly achieves steady-state regime, as scaling laws suggest (e.g. Breuer and Spohn, 2006; Stevenson, 2001). The general trend is that mantle heat flux decreases with time: rapidly during the Noachian, and more modestly afterwards. We assume that degree-one convection (Roberts and Zhong, 2007) produces partial melting and the source of water (Médard and Grove, 2006) beneath half of the planet (see Sections 4.2 and 4.3 for discussion). Serpentinization is then possible, depending on the crustal thermal gradient.

Assuming a given temperature at the base of the elastic thickness provides the thermal gradient. The interpretation of gravity and topographic data helps to estimate the elastic thickness of the lithosphere at the time the relief was formed. Values range between  $15$  to  $30 \text{ K km}^{-1}$

during the Early Noachian and decrease down to 5 to 15 K km<sup>-1</sup> at the Noachian/Hesperian limit (3.7 Ga). Choblet and Sotin (2001) find a rapid decrease from 30 K km<sup>-1</sup> after accretion down to 8 K km<sup>-1</sup> after 500 My of evolution. Their model assumes that heat is transferred by convection in the stagnant lid regime, like in our model, which implies very small lateral variations in heat flux. In this case, a viscosity of 10<sup>21</sup> Pa s gives a gradient of 2 K km<sup>-1</sup>, whereas 10<sup>18</sup> Pa s gives 20 K km<sup>-1</sup>. The latter value is in the range of the lower bound values derived by McGovern et al. (2004) and Grott et al. (2007). For a hotter crust, the trend of this gradient becomes highly non-linear, leading to a similar temperature difference in the Noachian martian crust to the linear case of our model, with an upper limit of 20 K km<sup>-1</sup>.

## 2.2. Composition, thickness and topography of the Noachian martian crust

The martian topographic dichotomy is similar to the ocean – continent difference on Earth. It corresponds to approximately 6 km of relief between the Northern lowlands and the Southern highlands (Fig. 1). An intriguing aspect is that there is no significant free-air gravity anomaly (or not correlated with topography) across this dichotomy (Yuan et al., 2001). The amplitude is about 0.001 m s<sup>-2</sup> (Fig. 1), which is on the order of a free-air gravity anomaly produced by a 1 km non-compensated topography contrast. It means that the 6 km martian topography contrast is mostly compensated either by different thicknesses of the same crust (known as Airy model) or by lateral variation in the composition of the crust (known as Pratt model).

The mineralogical composition of the martian surface has been investigated by the MGS Thermal Emission Spectrometer (TES) and the MEX Observatoire pour la Minéralogie, l'Eau, les Glaces et l'Activité (OMEGA) instruments. They have mapped mafic minerals – mainly pyroxenes, but also localized pure olivine outcrops – over the whole surface of Mars (Bandfield et al., 2000; Bibring et al., 2006; Hoefen et al., 2003; Mustard et al., 2005). *In-situ* measurements of the Mars Exploration Rovers (MERs) Spirit and Opportunity have revealed olivine in some exposed rocks of the lowlands (McSween et al., 2006). In addition, analyses of martian SNC meteorites argue in favor of a mafic composition for the martian crust (Nyquist et al., 2001). A contrast between a Southern basaltic, and a Northern andesitic crust was suggested by Bandfield et al. (2000), but this distinction was not observed in the MEX OMEGA data (Mustard et al., 2005). All these observations indicate a basaltic composition for the martian crust.

Assuming a homogeneous basaltic layer, estimates of the crustal thicknesses are 35 km in the Northern Hemisphere and 60 km in the Southern one (Wieczorek and Zuber, 2004). However, this thickness contrast may not be so important in the presence of a low-density rock layer in the Southern crust. Lower density serpentinized rocks can account for such a layer. Serpentine minerals have not been yet clearly observed on the surface of the Southern Hemisphere, even in large crater basins that should contain material of deeper serpentinized parts. But their weak reflectance (dark surface) precludes their detection by remote sensing methods. Nevertheless, the detection of pure olivine (Hoefen et al., 2003) and magnetite (Bertelsen et al., 2004) may suggest the presence of serpentine minerals.

In this study, we assume an initial basaltic homogeneous Noachian crust with constant thickness (Fig. 2). Then the lowest part of the Southern crust is serpentinized from its bottom toward the upper parts, because of the mantle water released by partial melting (cf. Section 2.1). The final hydrostatic equilibrium is expressed by:

$$(H_s + H_b - t)\rho_b = H_s\rho_s + H_b\rho_b \quad (1)$$

where  $H_s$  and  $H_b$  are the final thicknesses of the serpentinized and the non-serpentinized crusts, respectively (Fig. 2). A topography  $t$  is created at the surface to counterbalance the decrease in density from basalts ( $\rho_b = 3100$  kg m<sup>-3</sup>) to serpentinites ( $\rho_s = 2600$  kg m<sup>-3</sup>). Such a porous rock may exist even at large martian depths, because serpentinization creates

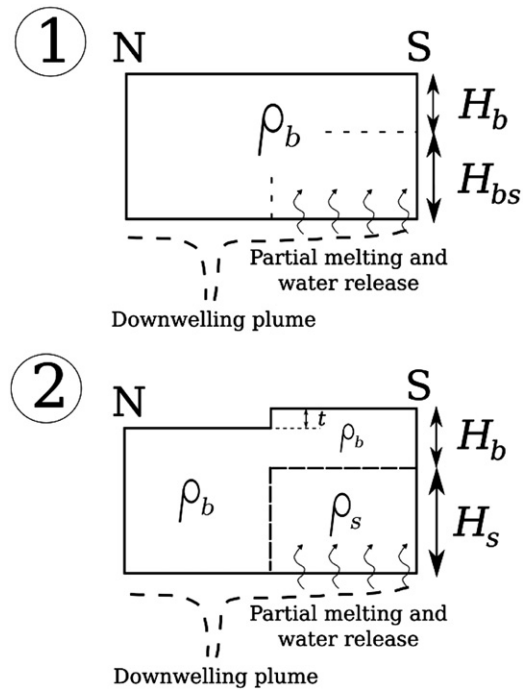


Fig. 2. Schematic N–S cross-section of the martian crust showing the initial (1) and final (2) compositions considered in this study. Volume masses for the serpentinized ( $\rho_s$ ) and basaltic ( $\rho_b$ ) crusts are 2600 and 3100 kg m<sup>-3</sup>, respectively. Indices for thicknesses correspond to Eq. (1)–(3):  $H_b$ , the thickness of the southern crust that will not be serpentinized (free parameter);  $H_{bs}$ , the thickness of the initial southern crust that will be serpentinized (31 km);  $H_s$ , the final thickness of the serpentinized crust in the Southern Hemisphere (37 km);  $t$ , the surface topography created during serpentinization (and increase of volume) of the lower crust (6 km).

its own porosity, allowing a continuous hydration (cf. Section 4.3). In Eq. (1), the Northern Hemisphere is represented on the left side, and the Southern one on the right side (Fig. 2). This approach allows us to estimate what is the minimum thickness of the serpentinized layer needed to reach the hydrostatic equilibrium. As a consequence, the initial thickness of the whole crust is not crucial, the only constraint is that it has to be large enough to produce a serpentinized layer, considering the thermodynamical conditions in the early martian crust. The thickness of the initial basaltic layer available for serpentinization,  $H_{bs}$ , is expressed by:

$$H_{bs} = H_s\rho_s/\rho_b \quad (2)$$

Then Eq. (1) is equivalent to:

$$H_{bs} = t\rho_s/(\rho_b - \rho_s) \quad (3)$$

Given the assumed densities, a 31.2 km – thick layer must be serpentinized to explain the present contrast of surface topography between the two hemispheres (6 km). Note that this scenario shows basalts still covering the whole surface of Mars, which correlates with observations. With Mars's mean radius of about 3390 km (as the actual one) and considering the Southern Hemisphere only, the material initially available for hydration then corresponds to  $2.23 \times 10^{18}$  m<sup>3</sup> of mafic rocks. Using other serpentinite densities of 2200 and 2800 kg m<sup>-3</sup>,  $H_{bs}$  ranges from 14.7 to 56.0 km, respectively.

The base of the serpentinized layer in the lower crust depends on the stability of the serpentine minerals. In our model, this limit needs to be deeper than 31.2 km. The thermodynamical conditions of several metamorphic reactions involving water and ultramafics are shown in Fig. 3, using data from Evans and Trommsdorf (1970) and Winkler (1979). A plot of several thermal gradients between 5 and 20 K km<sup>-1</sup> and

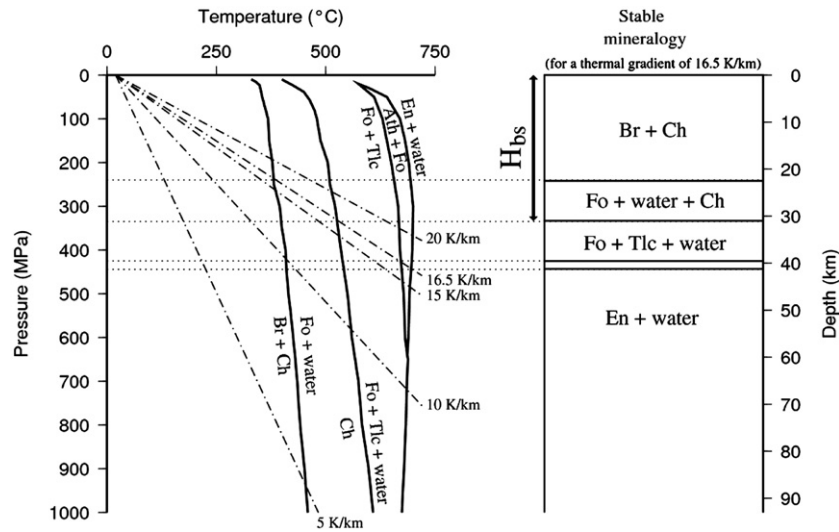


**Fig. 3.** Left: thermodynamical equilibrium of several reactions between ultramafics and water (solid lines) and thermal gradients (dot-dashed lines) with surface temperature of 293 K. Right: the associated mineralogy in the martian crust using a thermal gradient of 16.5 K km<sup>-1</sup>. Abbreviations: Br, Brucite; Ch, Chrysotile; Fo, Forsterite; Tlc, Talc; Ath, Anthophyllite; En, Enstatite; H<sub>bs</sub>, thickness of the initial crust that will be serpentinized (see Eq. (2) and Fig. 2).

using 293 K as surface temperature (as the present terrestrial mean surface temperature) reveals that the thermal gradient must be lower than 16.5 K km<sup>-1</sup> to let the serpentinization to reach 31.2 km. Otherwise, enstatite (as well as olivine for shallower depths) is stable as shown on the right panel of Fig. 3. If the assumed density is 2800 kg m<sup>-3</sup> (i.e. lower porosity), then the thermal gradient should be about 13 K km<sup>-1</sup>, which may be too low regards as the McGovern et al. (2004) and Grott et al. (2007)'s suggested ranges. Using a lower density up to 2200 kg m<sup>-3</sup>, it yields about 30 K km<sup>-1</sup>. Such large values have been suggested, but the used density would imply too large porosity for these depths. Thus, a density of 2600 kg m<sup>-3</sup> and H<sub>bs</sub> equal to 31.2 km for a thermal gradient of 16.5 K km<sup>-1</sup> is a compromised model. The latter value is consistent with the range of values we suggest in the previous Section 2.1. All

thermodynamical conditions in favor of serpentinization in the crust of the Southern Hemisphere were thus present during Noachian (see Sections 4.1 and 4.2 for discussion), creating density variations that explain the present gravity (compensation) and topography signals across the dichotomy.

### 3. Martian crustal magnetization via serpentinization

The serpentinization reactions are constrained by the thermodynamical conditions, by the rock bulk composition and available water volumes, as well as by the iron content in ultramafic minerals. Table 1 shows the selected mass-balanced reactions for this study. We only considered those which produce magnetite, where iron is exclusively

**Table 1**  
Serpentinization reactions considered in this study, with associated magnetization intensities

ID	Reactions of serpentinization <sup>a</sup>	Magnetization <sup>b</sup> (A m <sup>-1</sup> )
R01	30Fo <sub>95</sub> + 42.5H <sub>2</sub> O + 0.25CO <sub>2</sub> = 7.5Ch + 1Mt + 12Br + 0.25CH <sub>4</sub>	2.7
R02	30Fo <sub>90</sub> + 40H <sub>2</sub> O + 0.50CO <sub>2</sub> = 7.5Ch + 2Mt + 9Br + 0.50CH <sub>4</sub>	5.5
R03	30Fo <sub>85</sub> + 37.5H <sub>2</sub> O + 0.75CO <sub>2</sub> = 7.5Ch + 3Mt + 6Br + 0.75CH <sub>4</sub>	8.4
R04	30Fo <sub>80</sub> + 35H <sub>2</sub> O + 1CO <sub>2</sub> = 7.5Ch + 4Mt + 3Br + 1CH <sub>4</sub>	11.4
R05	30Fo <sub>75</sub> + 32.5H <sub>2</sub> O + 1.25CO <sub>2</sub> = 7.5Ch + 5Mt + 1.25CH <sub>4</sub>	14.5
R06	30Fo <sub>70</sub> + 27H <sub>2</sub> O + 1.5CO <sub>2</sub> = 6Ch + 6Mt + 3En <sub>100</sub> + 1.5CH <sub>4</sub>	18.3
R07	15En <sub>95</sub> + 19.25H <sub>2</sub> O + 0.125CO <sub>2</sub> = 4.75Ch + 0.5Mt + 11Q + 0.125CH <sub>4</sub>	2.1
R08	15En <sub>90</sub> + 25.33H <sub>2</sub> O + 3.67CO <sub>2</sub> = 4.5Ch + 1Mt + 12Q + 3.67CH <sub>4</sub>	4.1
R09	15En <sub>85</sub> + 17.75H <sub>2</sub> O + 0.375CO <sub>2</sub> = 4.25Ch + 1.5Mt + 13Q + 0.375CH <sub>4</sub>	6.3
R10	15En <sub>80</sub> + 22H <sub>2</sub> O + 3CO <sub>2</sub> = 4Ch + 2Mt + 14Q + 3CH <sub>4</sub>	8.4
R11	15En <sub>75</sub> + 16.25H <sub>2</sub> O + 0.625CO <sub>2</sub> = 3.75Ch + 2.5Mt + 15Q + 0.625CH <sub>4</sub>	10.6
R12	13.5En <sub>67</sub> + 13.5H <sub>2</sub> O + 0.75CO <sub>2</sub> = 3Ch + 3Mt + 15Q + 0.75CH <sub>4</sub>	14.3
R13	15Fo <sub>95</sub> + 2.5En <sub>85</sub> + 23.125H <sub>2</sub> O + 0.1875CO <sub>2</sub> = 5Ch + 0.75Mt + 2.75Br + 0.1875CH <sub>4</sub>	3.4
R14	6Fo <sub>95</sub> + 9.9En <sub>94</sub> + 20.3H <sub>2</sub> O + 0.15CO <sub>2</sub> = 5Ch + 0.6Mt + 5.8Q + 0.15CH <sub>4</sub>	2.6
R15	15Fo <sub>90</sub> + 5.25En <sub>85,7</sub> + 24.75H <sub>2</sub> O + 0.375CO <sub>2</sub> = 6Ch + 1.5Mt + 1.5Q + 0.375CH <sub>4</sub>	5.7
R16	6Fo <sub>90</sub> + 10.8En <sub>89</sub> + 20.6H <sub>2</sub> O + 0.3CO <sub>2</sub> = 5Ch + 1.2Mt + 7.6Q + 0.3CH <sub>4</sub>	4.9
R17	15Fo <sub>85</sub> + 6.375En <sub>82</sub> + 25.125H <sub>2</sub> O + 0.5625CO <sub>2</sub> = 6Ch + 2.25Mt + 3.75Q + 0.5625CH <sub>4</sub>	8.1
R18	6Fo <sub>85</sub> + 11.7En <sub>84,6</sub> + 20.9H <sub>2</sub> O + 0.45CO <sub>2</sub> = 5Ch + 1.8Mt + 9.4Q + 0.45CH <sub>4</sub>	7.0
R19	15Fo <sub>80</sub> + 4.5En <sub>67</sub> + 21.5H <sub>2</sub> O + 0.75CO <sub>2</sub> = 5Ch + 3Mt + 4Q + 0.75CH <sub>4</sub>	12.3
R20	6Fo <sub>80</sub> + 9.6En <sub>75</sub> + 17.2H <sub>2</sub> O + 0.6CO <sub>2</sub> = 4Ch + 2.4Mt + 9.2Q + 0.6CH <sub>4</sub>	10.9
R21	24Fo <sub>75</sub> + 0.75Fs + 26.25H <sub>2</sub> O + 1.125CO <sub>2</sub> = 6Ch + 4.5Mt + 1.5Q + 1.125CH <sub>4</sub>	15.7
R22	15Fo <sub>75</sub> + 5.625En <sub>67</sub> + 21.875H <sub>2</sub> O + 0.9375CO <sub>2</sub> = 5Ch + 3.75Mt + 6.25Q + 0.9375CH <sub>4</sub>	14.4
R23	6Fo <sub>75</sub> + 10.5En <sub>71</sub> + 17.5H <sub>2</sub> O + 0.75CO <sub>2</sub> = 4Ch + 3Mt + 11Q + 0.75CH <sub>4</sub>	12.8
R24	15Fo <sub>70</sub> + 3.75En <sub>40</sub> + 18.25H <sub>2</sub> O + 1.125CO <sub>2</sub> = 4Ch + 4.5Mt + 6.5Q + 1.125CH <sub>4</sub>	19.8
R25	6Fo <sub>70</sub> + 8.4En <sub>57</sub> + 13.8H <sub>2</sub> O + 0.9CO <sub>2</sub> = 3Ch + 3.6Mt + 10.8Q + 0.9CH <sub>4</sub>	18.2

<sup>a</sup> Abbreviations: Fo, Forsterite ((Mg,Fe)<sub>2</sub>SiO<sub>4</sub>); Ch, Chrysotile (Mg<sub>3</sub>Si<sub>4</sub>O<sub>10</sub>(OH)<sub>8</sub>); Mt, Magnetite (Fe<sub>3</sub>O<sub>4</sub>); Br, Brucite (Mg(OH)<sub>2</sub>); En, Enstatite ((Mg,Fe)<sub>2</sub>Si<sub>2</sub>O<sub>6</sub>); Q, Quartz (SiO<sub>2</sub>); Fs, Ferrosillite (Fe<sub>2</sub>Si<sub>2</sub>O<sub>6</sub>). Indices in Fo and En correspond to the magnesium content relative to iron (e.g. Fo<sub>75</sub> means (Mg<sub>0.75</sub>Fe<sub>0.25</sub>)<sub>2</sub>SiO<sub>4</sub>). Reactions R06 and R12 to R25 are in equilibrium with Br+Q=0.5 En<sub>100</sub>+water: therefore the iron content in the pyroxene differs from the one in olivine. Methane (CH<sub>4</sub>) is formed via dihydrogen (H<sub>2</sub>) and a Fischer-Tropsch typical reaction assuming the presence of CO<sub>2</sub>.

<sup>b</sup> Magnetization intensities are calculated via volume percentage of magnetite, magnetic susceptibility and assuming a surface magnetic field during magnetization of 50,000 nT.

stored. Therefore chrysotile is formed instead of lizardite, because the latter incorporates more iron in its structure than the former (O'Hanley and Dyar, 1993). Iron fraction in the initial olivine and pyroxene minerals varies from 5 to 30% (cf. Section 4).

For each reaction, the volume percentage of produced magnetite ( $V_{p_{Mt}}$ ) is computed using:

$$V_{p_{Mt}} = 100 \cdot n_{Mt} \cdot V_{Mt} / \sum (n_{Prod} \cdot V_{Prod}) \quad (4)$$

with  $n_{Mt}$ ,  $n_{Prod}$ ,  $V_{Mt}$  and  $V_{Prod}$  representing the numbers of moles and the molar volumes (in  $\text{m}^3 \text{mol}^{-1}$ ) of magnetite and other solid products of each reaction, respectively.

Based on magnetic measurements of serpentinized rocks, some authors proposed a linear relation between  $V_{p_{Mt}}$  and the magnetic susceptibility  $k$  (Oufi et al., 2002; Toft et al., 1990). The proportionality follows:

$$k \sim 0.03 \cdot V_{p_{Mt}} \quad (5)$$

In this way, the magnetic susceptibility of the rocks resulting from serpentinization reactions (listed in Table 1) is determined. The magnetization  $M$  (in  $\text{A m}^{-1}$ ) can be estimated from the magnetic field intensity  $B$  at the surface (in Tesla), following:

$$M = k \cdot B / \mu_0 \quad (6)$$

with  $\mu_0$  the magnetic permeability of free space ( $\mu_0 = 4\pi \times 10^{-7} \text{ H m}^{-1}$ ). The intensity of the magnetic field 4.0 Gy ago is poorly constrained for Mars as well as for the Earth (Prérot and Perrin, 1992). On average, the intensity of the martian remanent magnetic field is 10 to 100 times larger than the present terrestrial lithospheric field intensity. This implies either a stronger internal field responsible for rock magnetization at the surface, and/or a combination between a martian lithosphere enriched in magnetic material, and bearing minerals with higher magnetic susceptibility than on Earth. For convenience, a surface magnetic field of 50,000 nT is used, to be more easily compared to terrestrial rock magnetization (cf. Section 4). The resulting remanent magnetization intensities are shown in Table 1. They range from 2.1 to 19.8  $\text{A m}^{-1}$ , with an average of 9.7  $\text{A m}^{-1}$ . By comparison, a terrestrial rock is intensely magnetized when its magnetization exceeds 5  $\text{A m}^{-1}$ . Natural Remanent Magnetizations (NRM) of 5 to 20  $\text{A m}^{-1}$  are typically measured on mid-ocean ridge basalts and gabbros (Fox and Opdyke, 1973), although they decrease to less than 5  $\text{A m}^{-1}$  after a few million years due to the oxydation of magnetite into maghemite (Bleil and Petersen, 1983). Numerous studies reported that some oceanic serpentinized peridotites also possess quite large (more than 5  $\text{A m}^{-1}$ ) and stable NRM (see Oufi et al., 2002 and references therein). A more complex model may assume the serpentinization of such peridotites in the martian lithospheric mantle. The resulting magnetization would be deeper, but the heat flux

has to be lower. Other intense terrestrial NRM are also associated with continental volcanic formations (Gunnlaugsson et al., 2006), granulite rocks (McEnroe et al., 2001), as well as serpentinites (Lienert and Wasilewski, 1979).

The newly-formed magnetite changes from a superparamagnetic to a single-domain type during CRM acquisition. This CRM is very stable over geological times, with a relaxation time much greater than 100 My. Therefore there is no reason for an alteration of this CRM since the end of the Noachian period, assuming no significative thermal events have affected the martian crust during the last 3.7 Gy. On the other hand, the thermal state of the crust at the place of CRM acquisition could influence the resulting CRM intensity, which should decrease with depth (Dunlop and Özdemir, 1997). This could create vertical variations of the acquired CRM intensity that our model does not take into account. Alternatively, the estimated values of Table 1 may represent some averages of the total (or vertically integrated) magnetization inside the serpentinized layer, which only contributes to the magnetic measurements at satellite altitude. Finally, some of the previously mentioned terrestrial rocks are associated with large NRM even if they were magnetized in the lower crust, where the high temperature is expected to reduce the magnetization intensity of probable multi-domain newly-formed magnetite grains. Unfortunately, the current magnetization state of the martian crust is not constrained, because in-situ rock magnetization measurements do not exist. Particles of the martian soil and atmosphere are magnetic (Bertelsen et al., 2004), arguing for a significant magnetization of the martian regolith. The martian meteorites show quite weak associated magnetizations, except Los Angeles, NWA817 and NWA1068 (Rochette et al., 2001). One has thus to refer to estimations of the martian crustal magnetization derived from modeling of the MGS MAG/ER magnetic measurements. A summary of the published models is presented in Table 2. It clearly shows a variety of magnetization values, from 1 to 60  $\text{A m}^{-1}$ , most of the models predicting a mean crustal magnetization between 0 and 20  $\text{A m}^{-1}$ . This agrees very well with the magnetization obtained by our calculations based on chemical reactions of serpentinization (Table 1). Depending on the reaction, the resulting fraction of magnetite per volume of rocks ranges from 2.2 (for reaction R14) to 16.6% (for reaction R24), which is consistent with the observed magnetite content in terrestrial serpentinites (10–15%; Toft et al., 1990). Thus, in the presence of an intense magnetic field, production of magnetite through serpentinization may explain the intense magnetization that left its imprint on the early crust of Mars.

#### 4. Discussion

Our model depends on several assumptions about the early evolution of Mars. In the following, the compatibility of these hypotheses is

**Table 2**  
Models of the Martian crustal magnetization derived from MGS magnetic measurements

Authors	Crustal magnetization intensity ( $\text{A m}^{-1}$ )	Depth (km)	Location <sup>a</sup>
Connerney et al., 1999	20	0–30	T.C.
Sprenke and Baker, 2000	20	0–30	T.C.
Connerney et al., 2001	60	0–3	T.C.
Nimmo and Gilmore, 2001	40	0–10	T.S.T.C.
Frawley and Taylor, 2004	20	0–20	T.S.
Smrekar et al., 2004	9	0–10	I.A.
Langlais and Purucker, 2007	1 to 10	20	A.P.
Quesnel et al., 2007	>30	>30	T.S.
Purucker et al., 2000	0 to 20	0–50	Global
Arkani-Hamed, 2003	0 to 30	0–30	Global
Parker, 2003	>5	0–50	Global
Langlais et al., 2004	0 to 12	0–40	Global
Whaler and Purucker, 2005	0 to 20	0–40	Global

<sup>a</sup> Abbreviations: T.C., Terra Cimmeria; T.S., Terra Sirenum; I.A., Ismenius Area; A.P., Apollinaris Patera.

discussed considering the recent observations and the numerical modeling experiments that concern this topic.

#### 4.1. Pertinence of a stagnant lid convection regime during Noachian

The thermal gradient in the crust of Mars during Noachian resulted from the early thermal evolution of the whole planet. It is commonly assumed that, after accretion, the cooling of the magma ocean precedes the onset of mantle convection (Reese and Solomatov, 2006). During a short period, the core differentiation then buffers and homogenizes the mantle temperature with a cold layer on top. This evolution ends in a stagnant lid convection regime in the early Noachian, as suggested by Choblet and Sotin (2001). Recently, Guest and Smrekar (2007) showed that, if such a regime has occurred throughout the entire Mars's history, then a transition from a wet crust to a dry one is required at 3.5 Ga to preserve the dichotomy. The loss of the liquid water phase can be explained by serpentinization, even if, in our model, this process ends at ~4.0 Ga. The latter date also corresponds to the end of an efficient crustal production (Breuer and Spohn, 2006).

An alternative of the stagnant lid model is plate tectonics, as it has been proposed to explain the some magnetic anomalies (e.g. Connerney et al., 1999), and also invoked to generate sufficient heat flux out of the core to drive a convective dynamo (Nimmo and Stevenson, 2000). However, surface evidences for an episode of plate tectonics are lacking (Pruis and Tanaka, 1995; Zuber, 2001) and the timing of the interpreted transition to a stagnant lid regime is usually arbitrarily chosen to correlate with the apparent 500 Myr cessation of the dynamo. The absence of plate tectonics supports the preservation of the serpentinized layer in the martian crust through geological times which would otherwise be reduced by tectonic activity and recycling. Mars's mantle overturn is another possible scenario, but Guest and Smrekar (2007) show that it is strongly sensitive to the initial thermal conditions, and that such an event occurred too early in the Mars's history (50 Myr) to produce the observed magnetic anomalies.

#### 4.2. Hemispheric serpentinization and magnetization

The present model assumes mantle convection in the so-called stagnant lid regime. Both the cooling from above and internal heating favor instabilities of the cold thermal boundary layer beneath the conductive lid. Cold plumes are compensated by global upwelling of the warm mantle. Such a geometry favors global partial melting between the cold plumes. In addition, Zhong and Zuber (2001) and Roberts and Zhong (2007) showed that degree-one convection could be triggered at the core-mantle boundary, producing extensive partial melting in the head of a giant upwelling hot-plume. Such hot plume may have generated a consequent magmatic activity at the surface of Mars, initiating the growth of the Tharsis region. Assuming the contemporaneous serpentinization of the Southern crust (as in our model), different magnetization processes in the presence of a core dynamo would be implied: TRM for Tharsis volcanic rocks at surface, CRM for the serpentinized rocks in the lower crust. However, no intense magnetic anomalies were mapped over the Tharsis terranes. The reason could be either a less intense magnetization, or, more likely, that continuing volcanic activity subsequent to the dynamo shut-off have hidden some Noachian magnetized layers. This activity at Tharsis contributed to the crustal growth during Noachian and later. We exclude this contribution in our model and assume that serpentinization was the only crustal growth process during the end of the Noachian period (and no growth later). An alternate scenario may consist in a weak serpentinization of the Southern Hemisphere lower crust, allowing the remaining crust to be gradually thickened by continuous magmatism mainly during Noachian and Hesperian.

Excluding Tharsis and large crater basins, some areas of the Southern Hemisphere seem to be demagnetized (or weakly magnetized), e.g. from the west of Hellas to the east of Argyre. This contradicts our model,

which assumes a CRM by serpentinization in the whole crust beneath the current highlands. The apparent demagnetization may be of geological origin, because of the presence of shield volcanoes in this area. The dynamo regime (e.g. dipolar or not, with inversions or not) may also play a role (Stanley et al., 2008; Langlais and Amit, 2008).

We also would like to emphasize that a model with serpentinization occurring in the crust of both hemispheres may be possible. In such a scenario, the whole martian crust was magnetized by hydration during Noachian. Then, when the dynamo was extinct, demagnetization events (and thinning of the crust) happened in the Northern Hemisphere due to endogenic (subsequent hydrothermalism? mantle uplifting?) and/or exogenic (giant impact) processes (Watters et al., 2007). However, such a scenario needs to be constrained concerning the chronology of each event (before or after the end of the core dynamo?) and the part of the crust affected (lower or upper crust?).

Finally, the hypothesis of large-scale serpentinization – as considered in our model – is not well supported by terrestrial observations, which indicate specific geological settings such as the subduction zones or the mid-ocean ridges. However, our model shows ideal thermodynamical conditions in the entire Noachian martian Southern crust in favor of a possible large-scale process. Furthermore, using typical hydration reaction rates at large depths (~1000 m Myr<sup>-1</sup>; MacDonald and Fyfe, 1985; Ranero et al., 2003), the estimated timescale for this geological event fits the lifetime of the martian dynamo (~500 Ma; cf. Section 4.4.2).

#### 4.3. Surface vs. mantle origin for crustal water

The hydration of the martian crust at large depths was possible since the thermodynamical conditions favored serpentinization which renews the rock porosity by reducing the volume of liquid water plus solid olivine to solid chrysotile, as well as by creating cracks at small scale (O'Hanley, 1992; see also Vance et al., 2007). Even at low porosity conditions, this mechanism allowed a continuous hydration since it occurs preferentially along grain boundaries. Indeed, terrestrial serpentinization sites at large depths are observed by seismic experiments in forearc mantle of subduction zones (Ranero et al., 2003; Xia et al., 2008), as well as in the lower oceanic crust and mantle beneath slow-spreading ridges (Delescluse and Chamot-Rooke, 2008).

In our model, the water is abundant enough to alter the whole ultramafic minerals, creating  $2.63 \times 10^{18} \text{ m}^3$  of serpentinized crust ( $H_s = 37.2 \text{ km}$  in the Southern Hemisphere; cf. Eq. (1)–(3)). Typical concentration of water in serpentinites is about 12 wt.% (O'Hanley and Dyar, 1993). The corresponding mass of water trapped in this serpentinized crust would be equal to  $8.21 \times 10^{20} \text{ kg}$ , equivalent to a martian surface ocean of about 5.6 km thickness. It means that serpentinization has stored large quantities of the water released by partial melting of the upper mantle.

Médard and Grove (2006) estimate that more than 0.4 wt.% of water can be stored inside Mars during its accretion, which turns out to be about three times the amount necessary to serpentinized the crust. A significant amount of water was degassed during the differentiation of the planet, forming a wet atmosphere and eventually a hydrosphere. It may explain many topographical or geomorphological aspects of the old martian surfaces showing indices of liquid water runoff (e.g. Masson et al., 2001). Furthermore, MEX OMEGA (Bibring et al., 2006) and MERs (Ming et al., 2006) investigations have detected minerals reflecting aqueous alteration during Noachian times. Other numerical simulations of Mars's thermal evolution also predict significant amount of water released at this period by mantle degassing (e.g. Médard and Grove, 2006).

However, the nature and extension of this water reservoir remains unclear. If any wide area of liquid water really existed during Noachian at the surface of Mars, then it allowed hydrothermal convection in the upper crust. Oze and Sharma (2005) investigated this idea and considered a large serpentinization in the current martian crust, assuming that the water penetration may reach 25 km in depth. Such hydrothermalism is likely to preserve the crustal dichotomy through geological times (Parmentier and Zuber, 2007; Solomon et al., 2005).

However, if a global ocean serpentinized the crust from above in the two hemispheres, then no dichotomy would have been formed. And if a heterogeneous serpentinization led to form the dichotomy, then the water would have immediately moved toward the lowlands, stopping the serpentinization in the crust beneath the highlands. The observed directions of the Noachian valley networks are northward (Masson et al., 2001). Moreover, the presence of an ocean in the Northern Hemisphere was suggested to occur later, during the Hesperian period (Head et al., 1999), when the cratering rate was smaller. Even if hydration of the Northern Hemisphere crust might have taken place at that time, resulting magnetite did not acquire any coherent magnetization since the dynamo had already stopped. Therefore the present model with a serpentinization from the base of the conductive lid seems to better explain the observations and the formation of the dichotomy.

#### 4.4. The iron content, ancient core dynamo and paleo-magnetic field of Mars

Two primary factors control the magnetization associated with the serpentinization. These are the iron content of initial phases, and the magnetic field existing at the time of serpentinization. The more iron there is, and the more intense the ambient field is, the larger the magnetization is. Timing constraints for the dynamo shut-down are also needed to suggest that serpentinization only occurred during Noachian.

##### 4.4.1. Iron content

The serpentinization reactions listed in Table 1 use mafic minerals with iron content ranging from 5 to 30%. This range is consistent with the analyses of SNC meteorites (Nyquist et al., 2001), which give an iron bulk content equal to 25%. This is also compatible with the interpretation of physical properties of Mars (Mocquet et al., 1996; Sohl et al., 2005). Using measurements made by the MERs, McSween et al. (2006) identified iron-rich enstatite and olivine (Fo<sub>60-40</sub>) in the Gusev basalts. However, these rocks are thought to be of Hesperian age, younger than those which may have undergone serpentinization during Noachian. Martian meteorite ALH84001 contains orthopyroxene cumulate that crystallized 4.5 Ga ago. Its iron bulk content is 18.4%, with orthopyroxenes made of En<sub>68.8</sub> (Gleason et al., 1997). These values reinforce the hypothesis about the relatively high iron bulk content of the initial Martian lithosphere. Oze and Sharma (2007) mentioned that an initial iron content higher than 50% is not suited for serpentinization reactions, at least considering olivine as reactant. If the iron content is higher than 30%, then more magnetite is produced. Depending on the law to extrapolate the values derived in Table 1, a magnetization intensity range of 30–50 A m<sup>-1</sup> is expected for an initial iron content of 50%. These values are still in the range of published values for the martian crustal magnetization (Table 2). However, as shown by Oze and Sharma (2007), the probability of serpentinization reactions decreases from 0 to 50% of initial iron content, if olivine is the reactant. It thus leads to lower amounts of magnetite, which reduces the resulting magnetization to more commonly cited values, e.g. 0–20 A/m. Including more iron also affects the conditions of serpentinization occurrence. Winkler (1979) showed that 20% of iron in the starting mafic minerals decreases by 20 K the temperature of these reactions. In this case, the crustal model presented in Fig. 3 has to be modified towards a lower thickness for the serpentinized layer. Nevertheless, these changes are too small to significantly affect our calculations. Furthermore, the same model can be assumed using either a lower thermal gradient or a surface topography contrast less important. Therefore the assumed range of iron fraction in the mafic minerals is relevant.

##### 4.4.2. Timing of the martian core dynamo shut-down

In this study, we assume a Noachian core dynamo generated by a thermally driven core convection. We prefer this scenario as it

explains the apparent lack of magnetization associated with post-Noachian areas. In addition, it does not require the inception of an inner core (Stevenson, 2001). This idea is consistent with the current interpretation of the tidal Love number (Yoder et al., 2003), as well as with high-pressure-high-temperature experimental studies (Stewart et al., 2007), that Mars has a (partially or completely) liquid core. This also agrees with the high sulfur content (up to 14% by weight) in the martian core inferred from SNC meteorites (Dreibus and Wänke, 1985), because the presence of sulfur lowers the liquidus temperature and prevents a solid phase in a hot core. If the content of sulfur is lower, the inner core may start to freeze. However, the convection in the core is still prone to stop due to a diminishing heat flux outward the core and into the mantle due to the reduced efficiency of mantle cooling, leading to a thermally stratified core (Breuer and Spohn, 2006). In contrast, Schubert et al. (2000) assume an entirely solid martian core (or at least a significant inner solid shell) at present times. In their model, the onset of the magnetic field is postponed until a later stage (past ~4.0 Ga). However, the Noachian terranes and the >4.0 Ga old ALH84001 martian meteorite show remanent magnetization (Weiss et al., 2002), arguing for an early dynamo in the Mars's core.

##### 4.4.3. Intensity of the martian paleomagnetic field

We give in Table 1 magnetization values that would be associated with serpentinization processes occurring in the presence of a 50,000 nT magnetic field, as the mean field currently observed at the actual Earth's surface. Mafic minerals with a 20% Fe concentration lead to a 10 A m<sup>-1</sup> magnetization on average, while those with 30% Fe lead to 15 A m<sup>-1</sup>. These values are close to global magnetization models with a magnetized thickness of 40 km (Langlais et al., 2004; Whaler and Purucker, 2005). This may indicate that the paleomagnetic field at Mars surface was at maximum of the order of the actual terrestrial one.

Regardless of the nature of its driving forces, if the dynamo existed, its associated Elsasser number ( $\Lambda_E$ ), measuring the ratio of Lorentz to Coriolis forces, is written as:

$$\Lambda_E = \sigma B^2 / \rho \Omega \quad (7)$$

where  $\rho$  and  $\sigma$  are density and electrical conductivity of the core, respectively, and  $\Omega$  is the planetary rotation rate.  $B$  represents the magnetic field inside the core. In the so-called magnetostrophic regime, the Elsasser number is close to unity: Lorentz forces due to the motion of an electric current in the presence of a magnetic field are balanced by Coriolis forces due to the planetary rotation. Knowing  $\rho$ ,  $\sigma$  and  $\Omega$  allows to infer the strength of the magnetic field, using  $B \sim (\rho \Omega / \sigma)^{0.5}$ . On Earth, where  $\rho \approx 12,000 \text{ kg m}^{-3}$ ,  $\sigma \approx 5 \times 10^5 \text{ S m}^{-1}$  and  $\Omega = 7.292 \times 10^{-5} \text{ s}^{-1}$ , this scaling argument leads to a field value  $B_{Earth}$  of about  $1.323 \times 10^{-3} \text{ T}$ . The observed field value at the CMB (i.e. outside the core) is about 500,000 nT, which corresponds to an observed  $\Lambda_E$  of about 0.15. The difference between the expected and observed Elsasser number is explained by the lithospheric field overlapping the core field for high spherical harmonic degrees, and by the absence of information about the toroidal field contribution.

The same scaling argument is applied on Mars, where  $\Omega = 7.077 \times 10^{-5} \text{ s}^{-1}$ . Core density is estimated to  $7200 \text{ kg m}^{-3}$  (Sohl and Spohn, 1997). To estimate the electrical conductivity inside the martian core, we use a Wiedemann–Franz law and assume a thermal conductivity inside the martian core equal to  $40 \text{ W m}^{-1} \text{ K}^{-1}$  (Williams and Nimmo, 2004). Two-end member scenarios are considered, namely pure iron or Fe–FeS (14 wt.%) composition. For these two cases, the estimated mean temperature inside the martian core is 2400 K and 1850 K, respectively (Breuer and Spohn, 2006). We obtain electrical conductivity values ranging from  $4.6 \times 10^5$  to  $6.05 \times 10^5 \text{ S m}^{-1}$ , which correspond to a magnetic field strength in the martian core between  $1.052$  and  $0.918 \times 10^{-3} \text{ T}$ . These rough estimates show that under current conditions, the martian magnetic field inside the core would be slightly smaller (by about 30%) of the terrestrial one. This may not

be the case 4.0 Ga ago. It is also believed that the present rotation of Mars is very similar to its primordial one (Dehant et al., 2007). On the contrary, the Earth's rotation was faster than it is today, possibly down to 13 h (Williams, 2000). The associated magnetic field inside the Earth's core was then about  $1.795 \times 10^{-3}$  T, or 35% larger than the current day value.

Extrapolation of this core field to the surface is not straightforward, not only because of the non-visible part of the field (toroidal and lithospheric contributions), but also because the Earth's core was completely liquid (Labrosse et al., 2001). For our modeling purposes, we are going to use analogues of geomagnetic field strength determined from paleointensity measurements on terrestrial rocks. A caveat of our approach is that due to the metamorphic processes occurred throughout the geological time, the oldest terrestrial rocks that have been analyzed are Archean to Early Proterozoic in age (~3.5 to 2.5 Ga), younger than 4.0 Ga. However, it is assumed that their magnetization was acquired before the inner core started to solidify. Tarduno et al. (2007) recently reported values for paleofield between 20,000 and 60,000 nT, based on the analysis of Kaapvaal pluton (South Africa). Smirnov et al. (2003) reported similar values (43,000 nT) deduced from dikes in the region of Karela, Russia.

Elsasser number predicts a paleo-geomagnetic core field that was 1.35 times larger than it is today, while paleomagnetic studies see no significant differences between current and ancient geomagnetic fields. This may be due to the fact that the ratio of the toroidal to poloidal magnetic field was different, as a result of the absence of the inner core. Assuming similar ratios between core field and surface field on Mars and the Earth 4.0 Ga ago, a mean Earth's paleomagnetic field of 40,000 nT, a martian core field of the order of  $1 \times 10^{-3}$  T, a basic extrapolation predicts surface magnetic fields on Mars of the order of 25,000 nT. Such low fields are within the range deduced from ALH84001, between 0.1 and 1 times the present-day Earth's field (Weiss et al., 2002). In our study, we assumed a value of 50,000 nT for an easier comparison with the Earth. Our magnetization values (Table 1) have to be divided by 2, leading to a mean value of  $4.35 \text{ A m}^{-1}$ . This is consistent with values given in Table 2. For instance, Langlais et al. (2004) predicted a mean and maximum magnetization of 0.8 and  $12 \text{ A m}^{-1}$ , respectively. This mean value is for a 40-km thick layer over the whole martian surface. When reducing the thickness to 31.2 km, and considering only the highly-magnetized Terra Sirenum and Terra Cimmeria areas, the mean value is  $3 \text{ A m}^{-1}$ , very close to what we find here. This indicates that the large crustal magnetization of Mars does not mean that the magnetic field was intense.

#### 4.5. Implications for methane release

Methane can be produced through serpentinization when water contains  $\text{CO}_2$ , like in each reaction listed in Table 1. The presence and abundance of  $\text{CO}_2$  in crustal water depends on external and internal processes. Here we assume its presence and its reaction with the dihydrogen released by serpentinization. The maximum number of moles of methane produced via this process can be evaluated by assuming the initial content of ultramafic minerals. Using the initial volume of crust available for serpentinization ( $2.23 \times 10^{18} \text{ m}^3$ ; see Section 2), the production of methane through the reactions of Table 1 reaches about  $10^{21}$  mol. This has to be regarded as a maximum value because we consider that all the initial reactants are consumed. It does not compare with the less important amount previously proposed (see Krasnopolsky (2006) and references therein). Despite storage in the sub-surface crust via clathrates and photodissociation mechanisms, it indicates that methane, and maybe other complex organic molecules, may have been present in significant amount in the Noachian atmosphere.

## 5. Conclusions

In this study, the martian topographical and magnetization dichotomy is explained by assuming serpentinization of mafic rocks during the

Noachian. We demonstrate that Mars underwent favorable conditions for such a metamorphic process. The process proposed by our model only affects the actual Southern Hemisphere, and the associated decrease in density creates a topography between the two hemispheres that is consistent with the surface elevation difference of the martian dichotomy. Therefore it leads to no significant free-air gravity anomaly. Our scenario does not need an additional topography contrast at the base of the crust. Several reactions of serpentinization produce important quantities of magnetite which, in the presence of an Earth-like magnetic field, yield an associated magnetization in excellent agreement with crustal magnetization values derived from MGS measurements. The results also fit typical natural remanent magnetizations measured on terrestrial serpentinites. The absence of important amount of magnetite in the Northern Hemisphere crust can explain the fact that the lowlands lack or display weaker magnetic anomalies at the spacecraft altitude. Our model requires a core magnetic field at the time of serpentinization, and we show that the large martian crustal magnetization intensities do not mean that this paleo-magnetic field was intense.

To confirm that serpentinization happened during the Noachian period, several additional constraints are needed. One of these is to determine the exact thermodynamic conditions at which serpentinization can occur. Answers may come from sampling through dredging, diving and ocean drilling. Another aspect concerns the detection of serpentinized rocks in the present crust of Mars. The Compact Reconnaissance Imaging Spectrometer for Mars (CRISM) on-board Mars Reconnaissance Orbiter (MRO) has the ability to detect serpentine minerals at the Martian surface (Murchie et al., 2007). The MRO mission is also crucial to determine the exact composition of the crust, and thereafter, combining with gravimetric data, to explain the lack of gravity contrast between the two hemispheres. Last but not least, new magnetic field measurements at lower altitudes than MGS orbits are needed. The Mars Environment and Magnetic Orbiter (MEMO) mission was proposed in this way to ESA's Cosmic Vision program 2015–2025 (Langlais et al., 2008). Not only would such a mission give the first magnetic measurements around Mars since MGS, but also it is designed to study the current and past atmospheric escape.

## Acknowledgments

This paper benefited from a fruitful discussion with Pr. O. Oncken, M. Delescluse, J.-P. Valet, J.H. Roberts and S. Zhong, as well as from preliminary reviews of S. Vance and P. Rochette. This work was partly performed at the Jet Propulsion Laboratory, California Institute of Technology, under contract to the National Aeronautics and Space Administration.

## References

- Acuña, M.H., Connerney, J.E.P., Wasilewski, P., Lin, R.P., Mitchell, D., Anderson, K.A., Carlson, C.W., McFadden, J., Rème, H., Mazelle, C., Vignes, D., Bauer, S.J., Cloutier, P., Ness, N.F., 2001. Magnetic field of Mars: summary of results from the aerobraking and mapping orbits. *J. Geophys. Res.* 106, 23403–23417.
- Arkani-Hamed, J., 2003. Thermoremanent magnetization of the martian lithosphere. *J. Geophys. Res.* 108, 5114.
- Arkani-Hamed, J., 2005. On the possibility of single-domain/pseudo-single-domain magnetic particles existing in the lower crust of Mars: source of the strong magnetic anomalies. *J. Geophys. Res.* 110, E12009. doi:10.1029/2005JE002535.
- Arkani-Hamed, J., 2007. Magnetization of martian lower crust: revisited. *J. Geophys. Res.* 112, E05008. doi:10.1029/2006JE002824.
- Bandfield, J.L., Hamilton, V.E., Christensen, P.R., 2000. A global view of martian surface compositions from MGS-TES. *Science* 287, 1626–1630.
- Bertelsen, P., Goetz, W., Madsen, M.B., Kinch, K.M., Hviid, S.F., Knudsen, J.M., Gunnlaugsson, H.P., Merrison, J., Nornberg, P., Squyres, S.W., Bell, J.F., Herkenhoff, K.E., Gorevan, S., Yen, A.S., Myrick, T., Klingelhöfer, G., Rieder, R., Gellert, R., 2004. Magnetic properties experiments on the mars exploration rover spirit at Gusev Crater. *Science* 305, 827–829.
- Bibring, J.-P., Langevin, Y., Mustard, J.F., Poulet, F., Arvidson, R., Gendrin, A., Gondet, B., Mangold, N., Pinet, P., Forget, F., the OMEGA team, 2006. Global mineralogical and aqueous mars history derived from OMEGA/Mars Express Data. *Science* 312, 400–404.
- Blakely, R.J., Brocher, T.M., Wells, R.E., 2005. Subduction-zone magnetic anomalies and implications for hydrated forearc mantle. *Geology* 33, 445–448.

- Bleil, U., Petersen, N., 1983. Variations in magnetization intensity and low-temperature titanomagnetite oxidation of ocean floor basalts. *Nature* 301, 384–388.
- Breuer, D., Spohn, T., 2006. Viscosity of the martian mantle and its initial temperature: constraints from crust formation history and the evolution of the magnetic field. *Planet. Space Sci.* 54, 153–169.
- Choblet, G., Sotin, C., 2001. Early transient cooling of Mars. *Geophys. Res. Lett.* 28, 3035–3038.
- Connerney, J.E.P., Acuña, M.H., Wasilewski, P.J., Ness, N.F., Rème, H., Mazelle, C., Vignes, D., Lin, R.P., Mitchell, D.L., Cloutier, P.A., 1999. Magnetic lineations in the ancient crust of Mars. *Science* 284, 794–798.
- Connerney, J.E.P., Acuña, M.H., Wasilewski, P.J., Kletetschka, G., Ness, N.F., Rème, H., Lin, R.P., Mitchell, D.L., 2001. The global magnetic field of Mars and implications for crustal evolution. *Geophys. Res. Lett.* 28, 4015–4018.
- Dehant, V., Lammer, H., Kulikov, Y.N., Grießmeier, J.-M., Breuer, D., Verhoeven, O., Karatekin, Ö., Van Hoolst, T., Korabel, O., Lognonné, P., 2007. Planetary magnetic dynamo effect on atmospheric protection of early Earth and Mars. *Sp. Sci. Rev.* 129, 279–300.
- Delescluse, M., Chamot-Rooke, N., 2008. Serpentinization pulse in the actively deforming Central Indian Basin. *Earth Planet. Sci. Lett.* doi:10.1016/j.epsl.2008.09017.
- Dreibus, G., Wänke, H., 1985. Mars, a volatile-rich planet. *Meteoritics* 20, 367–381.
- Dunlop, D., Armani-Hamed, J., 2005. Magnetic minerals in the martian crust. *J. Geophys. Res.* 110 (E9). doi:10.1029/2005JE002404.
- Dunlop, D.J., Özdemir, Ö., 1997. *Rock Magnetism: Fundamentals and Frontiers*. Cambridge Univ. Press, New York, 573 pp.
- Evans, B.W., Trommsdorff, V., 1970. Regional metamorphism of ultramafic rocks in the Central Alps: paragenesis in the system CaO–MgO–SiO<sub>2</sub>–H<sub>2</sub>O. *Schweiz. Min. Petr. Mitt.* 50, 481–492.
- Fox, P.J., Opdyke, N., 1973. Geology of the oceanic crust: magnetic properties of oceanic rocks. *J. Geophys. Res.* 78, 5139–5154.
- Frawley, J.J., Taylor, P.T., 2004. Paleo-pole positions from martian magnetic anomaly data. *Icarus* 172, 316–327.
- Gleason, J.D., Kring, D.A., Hill, D.H., Boynton, W.V., 1997. Petrography and bulk chemistry of martian orthopyroxenite ALH84001: implications for the origin of secondary carbonates. *Geochim. Cosmochim. Acta* 61, 3503–3512.
- Grott, M., Hauber, E., Werner, S., Kronberg, P., Neukum, G., 2007. Mechanical modeling of thrust faults in the Thaumasia region, Mars, and implications for the Noachian heat flux. *Icarus* 186, 517–526.
- Guest, A., Smrekar, S.E., 2007. New constraints on the thermal and volatile evolution of Mars. *Phys. Earth Planet. Int.* 164, 161–176.
- Gunnlaugsson, H.P., Helgason, Ö.L., Kristjánsson, L., Nornberg, P., Rasmussen, H., Steinporsson, S., Weyer, G., 2006. Magnetic properties of olivine basalt: application to Mars. *Phys. Earth Planet. Int.* 154, 276–289.
- Harrison, K.P., Grimm, R.E., 2002. Controls on martian hydrothermal systems: application to valley network and magnetic anomaly formation. *J. Geophys. Res.* 107. doi:10.1029/2001JE001616.
- Head, J.W., Hiesinger, H., Ivanov, M., Kreslavsky, M.A., Pratt, S., Thomson, B.J., 1999. Possible ancient oceans on Mars: evidence from Mars orbiter laser altimeter data. *Science* 286, 2134–2137.
- Hess, H., 1962. History of ocean basins. In: Engel, A., James, H., Leonard, B. (Eds.), *Petrologic studies: a volume in honor of A.F. Geological Society of America, Buddington*. New York, pp. 599–620.
- Hoefen, T.M., Clark, R.N., Bandfield, J.L., Smith, M.D., Pearl, J.C., Christensen, P.R., 2003. Discovery of Olivine in the Nili Fossae region of Mars. *Science* 302, 627–630.
- Kletetschka, G., Wasilewski, P.J., Taylor, P.T., 2000. Unique thermoremanent magnetization of multidomain sized hematite: implications for magnetic anomalies. *Earth Planet. Sci. Lett.* 176, 469–479.
- Kletetschka, G., Ness, N.F., Connerney, J.E.P., Acuna, M.H., Wasilewski, P.J., 2005. Grain size dependent potential for self generation of magnetic anomalies on Mars via thermoremanent magnetic acquisition and magnetic interaction of hematite and magnetite. *Phys. Earth Planet. Int.* 148, 149–156.
- Korenaga, J., Jordan, T.H., 2002. Onset of convection with temperature- and depth-dependent viscosity. *Geophys. Res. Lett.* 29. doi:10.1029/2002GL015672.
- Krasnopolsky, V.A., 2006. Some problems related to the origin of methane on Mars. *Icarus* 180, 359–367.
- Labrosse, S., Poirier, J.-P., Le Mouél, J.-L., 2001. The age of the inner core. *Earth Planet. Sci. Lett.* 190, 111–123.
- Langlais, B., Purucker, M.E., 2007. A polar magnetic paleopole associated with Apollinaris Patera, Mars. *Planet. Space Sci.* 55, 270–279.
- Langlais, B., Amit, H., 2008. The past martian dynamo. *Science* 321, 1784–1785.
- Langlais, B., Purucker, M.E., Manda, M., 2004. Crustal magnetic field of Mars. *J. Geophys. Res.* 109, (E02008). doi:10.1029/2003JE002048.
- Langlais, B., Leblanc, F., Fouchet, T., Barabash, S., Breuer, D., Chassefière, E., Coates, A., Dehant, V., Forget, F., Lammer, H., Lewis, S., Lopez-Valverde, M., Manda, M., Menvielle, M., Pais, A., Paetzold, M., Read, P., Sotin, C., Tarits, P., Vennerstrom, S., Branduardi-Raymont, G., Cremonese, G., Merayo, J.G.M., Ott, T., Rème, H., Trotignon, J.G., Walhund, J.E., 2008. Mars environment and magnetic orbiter model payload. *Exp. Astron.* doi:10.1007/s10686-008-9101-1.
- Lienert, B.R., Wasilewski, P.J., 1979. A magnetic study of the serpentinization process at Burro Mountain, California. *Earth Planet. Sci. Lett.* 43, 406–416.
- MacDonald, A., Fyfe, W., 1985. Rate of serpentinization in seafloor environments. *Tectonophysics* 116, 123–135.
- Masson, P., Carr, M.H., Costard, F., Greeley, R., Hauber, E., Jaumann, R., 2001. Geomorphologic evidence for liquid water. *Space Sci. Rev.* 96, 333–364.
- McEnroe, S.A., Harrison, R.J., Robinson, P., Golla, U., Jercinovic, M., 2001. Effect of fine-scale microstructures in titanohematite on the acquisition and stability of natural remanent magnetization in granulite facies metamorphic rocks, southwest Sweden: implications for crustal magnetism. *J. Geophys. Res.* 106, 30523–30546.
- McGovern, P., Solomon, S., Smith, D., Zuber, M., Simons, M., Wieczorek, M., Phillips, R., Neumann, G., Aharonson, O., Head, J., 2004. Correction to “localized gravity/topography admittance and correlation spectra on Mars: implications for regional and global evolution”. *J. Geophys. Res.* 109, (E07007). doi:10.1029/2004JE002286.
- McSween, H.Y., Wyatt, M.B., Gellert, R., Bell III, J.F., Morris, R.V., Herkenhoff, K.E., Crumpler, L.S., Milam, K.A., Stockstill, K.R., Tornabene, L.L., Arvidson, R.E., Bartlett, P., Blaney, D., Cabrol, N.A., Christensen, P.R., Clark, B.C., Crisp, J.A., Des Marais, D.J., Economou, T., Farmer, J.D., Farrand, W., Ghosh, A., Golombek, M., Gorevan, S., Greeley, R., Hamilton, V.E., Johnson, J.R., Joliff, B.L., Klingelhofer, G., Knudson, A.T., McLennan, S., Ming, D., Moersch, J.E., Rieder, R., Ruff, S.W., Schröder, C., de Souza Jr., P.A., Squyres, S.W., Wänke, H., Wang, A., Yen, A., Zipfel, J., 2006. Characterization and petrologic interpretation of olivine-rich basalts at Gusev Crater, Mars. *J. Geophys. Res.* 111, (E02S10). doi:10.1029/2005JE002477.
- Médard, E., Grove, T.L., 2006. Early hydrous melting and degassing of the martian interior. *J. Geophys. Res.* 111, (E11003). doi:10.1029/2006JE002742.
- Mével, C., 2003. Serpentinization of abyssal peridotites at mid-ocean ridges. *C. R. Geoscience* 335, 825–852.
- Ming, D.W., Mittlefehldt, D.W., Morris, R.V., Golden, D.C., Gellert, R., Yen, A., Clark, B.C., Squyres, S.W., Farrand, W.H., Ruff, S.W., Arvidson, R.E., Klingelhofer, G., McSween, H.Y., Rodionov, D.S., Schröder, C., de Souza, P.A., Wang, A., 2006. Geochemical and mineralogical indicators for aqueous processes in the Columbia Hills of Gusev crater, Mars. *J. Geophys. Res.* 111. doi:10.1029/2005JE002560 (E02S12).
- Mocquet, A., Vacher, P., Grasset, O., Sotin, C., 1996. Theoretical seismic models of Mars: the importance of the iron content of the mantle. *Planet. Space Sci.* 44, 1251–1268.
- Morris, R.V., Ming, D.W., Graff, T.G., Arvidson, R.E., Bell III, J.F., Squyres, S.W., Mertzman, S.A., Gruener, J.E., Golden, D.C., Le, L., Robinson, G.A., 2005. Hematite spherules in basaltic tephra altered under aqueous, acid-sulfate conditions on Mauna Kea volcano, Hawaii: possible clues for the occurrence of hematite-rich spherules in the Burns formation at Meridiani Planum, Mars. *Earth Planet. Sci. Lett.* 240, 168–178.
- Murchie, S., Arvidson, R., Bedini, P., Beisser, K., Bibring, J.-P., Bishop, J., Boldt, J., Cavender, P., Choo, T., Clancy, R.T., Darlington, E.H., Des Marais, D., Espiritu, R., Fort, D., Green, R., Guinness, E., Hayes, J., Hash, C., Heffernan, K., Hemmler, J., Heyler, G., Humm, D., Hutcheson, J., Izenberg, N., Lee, R., Lees, J., Lohr, D., Malaret, E., Martin, T., McGovern, J.A., McGuire, P., Morris, R., Mustard, J., Pelkey, S., Rhodes, E., Robinson, M., Roush, T., Schaefer, E., Seagrave, G., Seelos, F., Silverglate, P., Slavney, S., Smith, M., Shyong, W.-J., Strohhahn, K., Taylor, H., Thompson, P., Tossman, B., Wirzburger, M., Wolff, M., 2007. Compact Reconnaissance Imaging Spectrometer for Mars (CRISM) on Mars Reconnaissance Orbiter (MRO). *J. Geophys. Res.* 112. doi:10.1029/2006JE002682 (E05S03).
- Mustard, J.F., Poulet, F., Gendrin, A., Bibring, J.-P., Langevin, Y., Gondet, B., Mangold, N., Bellugi, G., Altieri, F., 2005. Olivine and pyroxene diversity in the crust of Mars. *Science* 307, 1594–1597.
- Nimmo, F., 2000. Dike intrusion as a possible cause of linear martian magnetic anomalies. *Geology* 28, 391–394.
- Nimmo, F., Stevenson, D., 2000. Influence of early plate tectonics on the thermal evolution and magnetic field of Mars. *J. Geophys. Res.* 105, 11969–11979.
- Nimmo, F., Gilmore, M.S., 2001. Constraints on the depth of magnetized crust on Mars from impact craters. *J. Geophys. Res.* 106, 12315–12323.
- Nyquist, L.E., Bogard, D.D., Shih, C.-Y., Greshake, A., Stöffler, D., Eugster, O., 2001. Ages and geologic histories of martian meteorites. *Space Sci. Rev.* 96, 105–164.
- O’Hanley, D.S., 1992. Solution to the volume problem in serpentinization. *Geology* 20, 705–708.
- O’Hanley, D.S., Dyar, M.D., 1993. The composition of lizardite 1T and the formation of magnetite in serpentinites. *Am. Min.* 78, 391–404.
- Oufi, O., Cannat, M., Horen, H., 2002. Magnetic properties of variably serpentinized abyssal peridotites. *J. Geophys. Res.* 107. doi:10.1029/2001JB000549.
- Oze, C., Sharma, M., 2005. Have olivine, will gas: serpentinization and the abiogenic production of methane on Mars. *Geophys. Res. Lett.* 32. doi:10.1029/2005GL022691 (L10203).
- Oze, C., Sharma, M., 2007. Serpentinization and the inorganic synthesis of H<sub>2</sub> in planetary surfaces. *Icarus* 86, 557–561.
- Parker, R.L., 2003. Ideal bodies for Mars magnetism. *J. Geophys. Res.* 108. doi:10.1029/2001JE001760.
- Parmentier, E.M., Zuber, M.T., 2007. Early evolution of Mars with mantle compositional stratification or hydrothermal crustal cooling. *J. Geophys. Res.* 112. doi:10.1029/2005JE002626 (E02007).
- Prévot, M., Perrin, M., 1992. Intensity of the Earth’s magnetic field since Precambrian from Thellier-type palaeointensity data and inferences on the thermal history of the core. *Geophys. J. Int.* 108, 613–620. doi:10.1111/j.1365-246X.1992.tb04640.x.
- Pruis, M.J., Tanaka, K.L., 1995. The martian Northern plains did not result from plate tectonics. *Lunar Planet. Sci. XXVI*, 1147–1148.
- Purucker, M., Ravat, D., Frey, H., Voorhies, C., Sabaka, T., Acuna, M., 2000. An altitude-normalized magnetic map of Mars and its interpretation. *Geophys. Res. Lett.* 27, 2449–2452.
- Quesnel, Y., Langlais, B., Sotin, C., 2007. Local inversion of magnetic anomalies: implication for Mars crustal evolution. *Planet. Space Sci.* 55, 258–269.
- Ranero, C., Phipps Morgan, J., McIntosh, K., Reichert, C., 2003. Bending-related faulting and mantle serpentinization at the Middle America trench. *Nature* 425, 367–373.
- Reese, C.C., Solomatov, V.S., 2006. Fluid dynamics of local martian magma oceans. *Icarus* 184, 102–120.
- Roberts, J.H., Zhong, S., 2007. The cause for the north-south orientation of the crustal dichotomy and the equatorial location of Tharsis on Mars. *Icarus* 190, 24–31.
- Rochette, P., Lorand, J.-P., Fillion, G., Sautter, V., 2001. Pyrrhotite and the remanent magnetization of SNC meteorites: a changing perspective on martian magnetism. *Earth Planet. Sci. Lett.* 190, 1–12.
- Schubert, G., Russell, C.T., Moore, W.B., 2000. Timing of the martian dynamo. *Nature* 408, 666–667.

- Shahnas, H., Arkani-Hamed, J., 2007. Viscous and impact demagnetization of martian crust. *J. Geophys. Res.* 112. doi:10.1029/2005JE002424 (E02009).
- Smirnov, A.V., Tarduno, C.J., Pisakin, B.N., 2003. Paleointensity of the early geodynamo (2.45 Ga) as recorded in Karelia: a single-crystal approach. *Geology* 31, 415–418.
- Smith, D.E., Zuber, M.T., Solomon, S.C., Phillips, R.J., Head, J.W., Garvin, J.A., Banerdt, W.B., Muhleman, D.O., Pettengill, G.H., Neumann, G.A., Lemoine, F.G., Abshire, J.B., Aharonson, O., Brown, C.D., Hauck, S.A., Ivanov, A.B., McGovern, P.J., Zwally, H.J., Duxbury, T.C., 1999. The global topography of Mars and implications for surface evolution. *Science* 284, 1495–1503.
- Smrekar, S.E., McGill, G.E., Raymond, C.A., Dimitriou, A.M., 2004. Geologic evolution of the martian dichotomy in the Ismenius area of Mars and implications for plains magnetization. *J. Geophys. Res.* 109. doi:10.1029/2004JE002260 (E11002).
- Sohl, F., Spohn, T., 1997. The interior structure of Mars: implications from SNC meteorites. *J. Geophys. Res.* 102, 1613–1635.
- Sohl, F., Schubert, G., Spohn, T., 2005. Geophysical constraints on the composition and structure of the martian interior. *J. Geophys. Res.* 110. doi:10.1029/2005JE002520 (E12008).
- Solomon, S.C., Aharonson, O., Aurnou, J., Banerdt, W.B., Carr, M.H., Dombard, A.J., Frey, H.V., Golombek, M.P., Hauck II, S.A., Head III, J.W., Jakosky, B.M., Johnson, C.L., McGovern, P.J., Neumann, G.A., Phillips, R.J., Smith, D.E., Zuber, M.T., 2005. New perspectives on ancient Mars. *Science* 307, 1214–1220.
- Sprenke, K.F., Baker, L.L., 2000. Magnetization, paleomagnetic poles, and polar wander on Mars. *Icarus* 147, 26–34.
- Stanley, S., Elkins-Tanton, L., Zuber, M.T., Parmentier, E.M., 2008. Mars paleomagnetic field as the result of a single-hemisphere dynamo. *Science* 321, 1822–1825.
- Stevenson, D.J., 2001. Mars core and magnetism. *Nature* 412, 214–219.
- Stewart, A.J., Schmidt, M.W., van Westrenen, W., Liebske, C., 2007. Mars: a new core-crystallisation regime. *Science* 316, 1323–1325.
- Tarduno, J.A., Cottrell, R.D., Watkeys, M.K., Bauch, D., 2007. Geomagnetic field strength 3.2 billion years ago recorded by single silicate crystals. *Nature* 446, 657–660.
- Toft, P.B., Arkani-Hamed, J., Haggerty, S.E., 1990. The effects of serpentinization on density and magnetic susceptibility: a petrophysical model. *Phys. Earth Planet. Int.* 65, 137–157.
- Vance, S., Harnmeijer, J., Kimura, J., Hussmann, H., deMartín, B., Brown, J.M., 2007. Hydrothermal Systems in Small Ocean Planets. *Astrobiology* 7 (6). doi:10.1089/ast.2007.0075.
- Watters, T.R., McGovern, P.J., Irwin III, R.P., 2007. Hemispheres apart: the crustal dichotomy on Mars. *Annu. Rev. Earth Planet. Sci.* 35, 621–652.
- Weiss, B.P., Vali, H., Baudenbacher, F.J., Kirschvink, J.L., Stewart, S.T., Schuster, D.L., 2002. Record of an ancient martian magnetic field in ALH84001. *Earth Planet. Sci. Lett.* 201, 449–463.
- Whaler, K.A., Purucker, M.E., 2005. A spatially continuous magnetization model for Mars. *J. Geophys. Res.* 110. doi:10.1029/2004JE002393 (E09001).
- Wieczorek, M.A., Zuber, M.T., 2004. Thickness of the martian crust: improved constraints from geoid-to-topography ratios. *J. Geophys. Res.* 109. doi:10.1029/2003JE002153 (E01009).
- Williams, G.E., 2000. Geological constraints on the Precambrian history of Earth's rotation and the Moon's orbit. *Rev. Geophys.* 38, 37–59.
- Williams, J.-P., Nimmo, F., 2004. Thermal evolution of the martian core: implications for an early dynamo. *Geology* 32, 97–100.
- Winkler, H.G.F., 1979. *Petrogenesis of Metamorphic Rocks*, fifth ed. Springer-Verlag, New York, Heidelberg, Berlin.
- Xia, S., Zhao, D., Qiu, X., 2008. Tomographic evidence for the subducting oceanic crust and forearc mantle serpentinization under Kyushu, Japan. *Tectonophysics* 449, 85–96.
- Yoder, C.F., Konopliv, A.S., Yuan, D.N., Standish, E.M., Folkner, W.M., 2003. Fluid core size of Mars from detection of the solar tide. *Science* 300, 299–303.
- Yuan, D., Sjogren, W.L., Konopliv, A.S., Kucinskis, A.B., 2001. Gravity field of Mars: a 75th degree and order model. *J. Geophys. Res.* 106, 23377–23402.
- Zhong, S., Zuber, M.T., 2001. Degree-1 mantle convection and the crustal dichotomy on Mars. *Earth Planet. Sci. Lett.* 189, 75–84.
- Zuber, M.T., 2001. The crust and mantle of Mars. *Nature* 412, 220–227.